Published in final edited form as:
Mol Imaging Biol. 2013 October ; 15(5): 507–520. doi:10.1007/s11307-013-0648-5.

Pharmacokinetic Issues of Imaging with Nanoparticles: Focusing on Carbon Nanotubes and Quantum Dots

Hao Hong[1,4], **Feng Chen**[1,4], and **Weibo Cai**[1,2,3,*]

[1]Department of Radiology, University of Wisconsin - Madison, WI, USA

[2]Department of Medical Physics, University of Wisconsin - Madison, WI, USA

[3]University of Wisconsin Carbone Cancer Center, Madison, WI, USA

Abstract

With many desirable properties, nanoparticles hold tremendous potential for non-invasive molecular imaging and improving the efficacy of small molecule drugs. The pharmacokinetics (PK) and tissue distribution of nanoparticles largely define their *in vivo* performance and potential toxicity, which are fundamental issues that need to be elucidated. In this review article, we summarized how molecular imaging techniques (e.g. positron emission tomography, fluorescence imaging, etc.) can facilitate the investigation of PK profiles of nanoparticles, using carbon nanotubes (CNTs) and quantum dots (QDs) as representative examples. Different imaging techniques can provide useful insights in monitoring the *in vivo* behavior and tissue distribution of these nanoparticles, and a number of strategies were employed to improve the PK profiles of CNTs and QDs. Based on the available literature reports, it can be concluded that chemical and physical properties of the nanoparticles (e.g. surface functionalization, hydrodynamic size, shape, surface charge, etc.), along with the administration routes/doses, can play important roles in determining the PK and biodistribution pattern of nanoparticles. Robust chemistry for surface modification of nanoparticles is the key to success in future biomedical and clinical applications.

Keywords

Pharmacokinetics (PK); molecular imaging; nanoparticles; carbon nanotube (CNT); quantum dot (QD); cancer; angiogenesis; positron emission tomography (PET); fluorescence

INTRODUCTION

Nanotechnology, an interdisciplinary research field involving physics, chemistry, engineering, biology, material science, medicine, among others, has great potential for early detection, accurate diagnosis, and personalized treatment of diseases [1–3]. A wide variety of nanoparticles have been investigated for the delivery of drugs, where improved tissue selectivity could be achieved due to selective uptake of nanoparticles in certain tissues. The pharmacokinetic (PK) profiles of the “free” drug and the drug encapsulated in the nanoparticles are often different. Therefore, it is very important to monitor the PK and biodistribution of nanoparticles to understand and predict their efficacy and potential side effects [4]. PK is defined as the science of quantifying the rate and extent of absorption,

Requests for reprints: Weibo Cai, PhD, Departments of Radiology and Medical Physics, University of Wisconsin - Madison, Room 7137, 1111 Highland Avenue, Madison, WI 53705-2275, USA, wcai@uwhealth.org; Phone: 608-262-1749; Fax: 608-265-0614.
[4]Contributed equally to this work

Conflict of Interest. The authors declare that they have no conflict of interest.

distribution, metabolism, and elimination (ADME) of chemicals and drugs in the body. Some of the most important parameters in PK include C_{max} (maximum concentration), $t_{1/2}$ (half-life), clearance, area under the curve (AUC), and mean resident time (MRT; i.e. average time that the drug molecule stays inside the body).

The PK of nanoparticles is controlled by a complex array of interrelated physicochemical and biological factors, and in-depth knowledge of the particle characteristics (both before and after administration into living subjects) is critical for optimal performance of the nanoparticles as drug carriers and/or imaging agents. Currently, there is a lack of techniques available to assess, measure, and follow real-time events pertaining to nanoparticle characteristics in the circulation and after extravasation (e.g., flow properties within the blood vessels, plasma protein binding dynamics, dynamic size and shape changes, excretion/redistribution profiles, etc.).

One of the most useful tools to assess the PK of nanoparticles is molecular imaging, “the visualization, characterization and measurement of biological processes at the molecular and cellular levels in humans and other living systems” [5–7]. Over the last decade, a wide variety of nanoparticles have been investigated with molecular imaging techniques [8–10]. In this review article, we aim to provide a brief overview on how molecular imaging techniques can facilitate the study of the PK of nanoparticles, using carbon nanotubes (CNTs) and quantum dots (QDs) as two representative examples. Although comprehensive investigation is still needed in future research of nanoparticle-based imaging/therapeutic agents, it is clear that molecular imaging can serve as indispensable tools for PK studies of various nanoparticles.

PK OF CNTS

Carbon nanotubes, including single-walled carbon nanotubes (SWNTs) and multi-walled carbon nanotubes (MWNTs), have shown great promises in many research areas especially biomedicine [11–12]. Functionalized CNTs are reported to be capable of shuttling various biomolecules into cells effectively, including drugs, plasmid DNA, small interfering RNA, etc. [12–14]. In addition, encouraging results for CNT-based cancer therapy has been achieved in various small animal models *in vivo*.

Although a number of literature reports from many research groups have shown promising results of CNT-based nanomedicine, much future effort will be needed before these exciting findings can be translated into the clinic to benefit cancer patients. The PK, long-term fate, and potential toxicity of CNTs should be thoroughly examined before the ultimate applications of CNT-based agents in the clinic [3, 15]. Over the last decade, many studies have been carried out to assess the PK, biodistribution, and toxicity of CNTs in animals [16–20]. Various imaging techniques have been employed to study the *in vivo* behavior of CNTs, which include radionuclide-based techniques such as positron emission tomography (PET) and single-photon emission computer tomography (SPECT), optical imaging (e.g. with fluorescence and Raman detection), photoacoustic imaging (PAI), magnetic resonance imaging (MRI), etc. In the next section, we summarize the findings regarding PK of CNTs and clarify the important factors that affect the *in vivo* behavior and toxicology of CNTs.

Imaging CNTs with various techniques

Radionuclide-based imaging—Radionuclide-based imaging techniques have been widely used in clinical oncology over the last several decades [21–25]. Since PET and SPECT imaging are sensitive and quantitative, radiolabeling has often been employed to evaluate the PK of CNTs. To date, many radioisotopes have been used for *in vivo* tracking

of CNTs with SPECT and PET, such as ^{111}In ($t_{1/2}$: 67.5 h), 125I ($t_{1/2}$: 60 d), 64Cu ($t_{1/2}$: 12.7 h), 86Y ($t_{1/2}$: 14.7 h), and 89Zr ($t_{1/2}$: 78.4 h).

The distribution profile of ^{111}In-labeled MWNTs and SWNTs was monitored by SPECT [26–27]. Rapid renal excretion of the labeled CNTs was reported, which was attributed to the one-dimensional shape of these CNTs. In another study, a similar labeling strategy was used to investigate whether antibody conjugation onto the SWNTs could confer enhanced tumor accumulation in mouse models [28]. Encouraging results were observed for specific tumor targeting with these antibody-conjugated CNT constructs both *in vitro* and *in vivo*.

Besides ^{111}In, ^{125}I has also been used to label CNTs and evaluate their *in vivo* kinetics. For example, water-soluble hydroxylated SWNTs were labeled with ^{125}I to study the distribution in mice [29]. It was suggested that these SWNTs moved easily among the compartments and tissues of the body and behaved as small molecules, although their apparent molecular weight is tremendously large. However, the high uptake of ^{125}I in the stomach suggested significant deiodination from the labeled SWNTs, therefore the distribution of ^{125}I may not accurately reflect the distribution of SWNTs *in vivo*. In order to reduce deiodination, ^{125}I encapsulation (i.e. Na^{125}I was sealed inside the SWNTs, which were subsequently covalently modified with biantennary carbohydrates) was conducted in another report to study the distribution of glycosylated SWNTs (termed as GlcNAc^{D}-Na^{125}I@SWNTs) in mice after intravenous administration [30]. Specific accumulation was observed in the mouse lung (Figure 1), which confirmed high *in vivo* stability of GlcNAc^{D}-Na^{125}I@SWNTs. This labeling method prevented leakage of radionuclide to high-affinity organs (e.g. ^{125}I to the thyroid and stomach) or excretion, and resulted in sensitive and longitudinal tracking of the ^{125}I-labeled SWNTs for up to 7 days. Clearance of the ^{125}I-labeled SWNTs via liver and kidney was observed.

In one early study, the biodistribution in mice of ^{64}Cu-labeled SWNTs, which were functionalized with polyethylene glycol (PEG) chains of different length on the SWNT surface (2 kDa or 5.4 kDa), was investigated [31]. It was found that these SWNT conjugates were highly stable *in vivo* and the surface PEG chain length could significantly affect the circulation half-life and biodistribution. Both SWNT conjugates showed significant accumulation in the mononuclear phagocyte system (MPS), and significantly reduced MPS uptake was observed for SWNTs coated with longer PEG chains (i.e. 5.4 kDa). Importantly, efficient targeting of integrin $\alpha_v\beta_3$-positive tumors in mice was achieved with SWNTs coated with 5.4 kDa PEG chains, when a cyclic arginine-glycine-aspartic acid (RGD, potent antagonist of integrin $\alpha_v\beta_3$ [32]) peptide was used as the targeting ligand.

In another report, ^{86}Y-DOTA-SWNTs (DOTA denotes 1,4,7,10-tetraazacyclododecane-1,4,7,10-tetraacetic acid) were synthesized and the whole-body distribution and clearance were investigated by PET [33]. It was reported that ^{86}Y-DOTA-SWNTs cleared from the blood within 3 hours and distributed predominantly to the kidneys, liver, spleen, and bone. Although radioactivity in the kidney cleared with time, whole-body clearance of ^{86}Y-DOTA-SWNTs was slow. Over the last decade, ^{89}Zr has been extensively investigated for antibody labeling and PET imaging [34–35]. Using desferrioxamine as the chelator, ^{89}Zr-labeled SWNTs were prepared and investigated in LS174T tumor-bearing mice with serial PET imaging [36]. Rapid blood clearance (< 1 h) and specific tumor accumulation of the construct was observed.

Radiolabeling with PET/SPECT isotopes is highly sensitive for investigating the PK of CNTs. However, one major concern is the potential detachment of radioisotopes from CNTs inside the animal body, which can cause misleading findings since PET/SEPCT imaging detects the radioisotopes (whether they are on the CNTs or not) but not the CNTs

themselves. High *in vivo* stability of the radiolabeled CNTs is critical for long-term tracking and excretion studies. Besides the abovementioned positron-emitting and gamma-emitting isotopes, another alternative for labeling CNTs is ^{14}C ($t_{1/2}$: 4370 y). In one study, 14C-labeled MWNTs (functionalized by ^{14}C-taurine) were prepared to study the biodistribution and translocation pathways of MWNTs in mice through *ex vivo* autoradiography [37], where persistent liver accumulation was observed for over one month. Subsequently, the ^{14}C-labeling strategy was further optimized for MWNTs by generating a C-C bond between MWNTs and the ^{14}C [38]. The highly stable C-C bond makes the distribution profile (based on ^{14}C detection) more reliable, and the organs with prominent accumulation of ^{14}C-labeled MWNTs were found to be the liver, lung, and spleen (Figure 2). Slow excretion of the MWNTs from mice was also noticed in this study.

Imaging CNTs with their intrinsic properties—Despite the high sensitivity of radionuclide-based imaging techniques, complete elimination of radioisotope detachment from labeled CNTs is challenging, even with ^{14}C-labeling. In the meantime, CNTs possess many unique intrinsic physical properties, which can be extremely useful for their *in vivo* and/or *ex vivo* long-term tracking. For example, the intrinsic near-infrared fluorescence (NIRF) signal suggests that CNTs may be useful fluorescent tags for imaging applications in small animal studies. However, the extremely low quantum yield and high sensitivity to environmental conditions make NIRF imaging of CNTs very challenging. In one report, the inherent NIRF signal of SWNTs were used to study the biodistribution in rabbits [18]. Individualized, chemically pristine SWNTs were intravenously administered to rabbits and monitored ex vivo through their characteristic NIRF signal in the blood sample and excised tissue. Similar as observed in many other literature reports, these SWNTs were found to mostly accumulate in the liver. Generally speaking, NIRF imaging of CNTs is not ideal for quantitative measurement and long-term tracking *in vivo*.

Raman spectroscopy, which can differentiate the spectral fingerprint of many molecules [10, 39], can serve as another important tool for imaging of SWNTs. SWNTs have an intense Raman peak produced by strong electron-phonon coupling, which causes efficient excitation of tangential vibration in the SWNT upon light exposure [40]. In a pioneering study, SWNTs and other nanoparticles were studied for their potential in non-invasive Raman imaging, PK evaluation, multiplexing, as well as *in vivo* tumor targeting, with an imaging system adapted for small animal Raman imaging [41]. In the meantime, another study used Raman spectroscopy to quantitatively measure the concentration of intravenously injected SWNTs in various organs and tissues of mice ex vivo over a period of three months [16]. Near-complete disappearance of SWNT Raman signal was observed after three months (Figure 3).

Shortly after these reports, an optimized Raman microscope was developed to evaluate tumor targeting and localization of SWNTs in tumor-bearing mice [42]. In addition, the acute and chronic toxicity of functionalized SWNTs were examined by Raman microscopy and histology for over four months, after intravenous injection into mice [17]. The Raman signal of SWNTs was very stable against photobleaching, thereby enabling long-term imaging and tracking. No obvious toxic effect was observed in mice, which paved the way for future investigation of SWNT-based agents for various biomedical applications such as cancer imaging and therapy. The primary limitations of Raman imaging in larger subjects are those also faced by other optical techniques: even in the near-infrared region (700–900 nm), light penetration beyond a few centimeters of tissue is very challenging [43–45]. The key advantages of Raman imaging over fluorescence imaging is the superb multiplexing capability and lack of confounding background signal from tissue autofluorescence.

PAI is an imaging technique based on the photoacoustic effect in which the tissue is usually irradiated by a short-pulsed laser beam to produce thermal and acoustic responses (i.e. light in, sound out) [46–48]. PAI can offer higher spatial resolution and slightly better tissue penetration than most other optical imaging techniques. SWNT conjugated with cyclic RGD peptides was first reported as a molecularly-targeted contrast agent for PAI in tumor-bearing mice [49], and the detection limit of PAI for SWNTs was reported to be ~50 nM in this study. One of the major limitations of this imaging technique is that the data acquisition time was quite long, therefore it may not be an ideal choice for *in vivo* evaluation of the PK of SWNTs. Subsequently, it was demonstrated that indocyanine green-enhanced SWNTs could generate about 300 times higher photoacoustic contrast than the abovementioned SWNTs [50]. Recently, a photoacoustic microscope was developed to detect trace amount of SWNTs in tissue specimens, which may be used for future PK evaluation of SWNTs [51].

MRI—MRI detects the interaction of protons (or certain other nuclei) with each other and with the surrounding molecules in a tissue of interest [52–53]. Development of Gd^{3+}-functionalized SWNTs for MRI applications has been reported [54], and the distribution pattern of Gd^{3+}-doped SWNTs after the release from a degrading poly(lactic-co-glycolic acid) (PLGA) scaffold was studied in rats [55]. The release of Gd^{3+}-SWNTs from the PLGA scaffold into the surrounding tissue was observed during a period of three weeks. In several other studies, susceptibility-weighted MRI was adopted to evaluate the distribution of raw and purified SWNTs [19, 56]. The susceptibility effects induced by metal impurity in the intrapulmonary instilled raw SWNT samples were large enough to cause a significant drop in magnetic field homogeneity, which was detectable by MRI. Of note, this technique is not suitable for monitoring the PK of ultra-pure, robustly surface-functionalized SWNTs.

Other techniques—One of the most direct measurements of SWNT biodistribution was reported in 2007 [57]. In this study, the biodistribution of pristine SWNTs in mice was determined by using the skeleton ^{13}C-enriched SWNTs and isotope ratio mass spectroscopy (which measures the $^{13}C/^{12}C$ ratios). The concentration of ^{13}C-enriched SWNTs in various organs was determined and the results suggested that these SWNTs were distributed in the entire mouse body, with major accumulation in the liver, lungs, and spleen over an extended period of time (without appreciable clearance over 28 days). Although such measurement of $^{13}C/^{12}C$ ratios is direct and unbiased, the requirement of special sample preparation (e.g. ^{13}C enrichment) and low detection sensitivity are major disadvantages for this approach. Recently, dual-modality optical coherence tomography (OCT) and MRI was also investigated for detection of PEG-coated SWNTs in aqueous solutions [58]. However, no *in vivo* studies were reported.

Major factors that affect the PK of CNTs

PK is a critically important factor to determine the therapeutic efficacy of a drug or the *in vivo* performance of an imaging agent. Although much more systematic research will need to be performed in the future to thoroughly characterize the PK of SWNTs and MWNTs in small and large animals before potential clinical applications, some general principles can be gleaned from the available literature reports. Because direct comparison of results from literature reports is very challenging due to the different CNTs, animal species, animal models, etc. that were employed for each individual investigation, these general principles may not apply to all CNT-based imaging/therapeutic agents and case-by-case evaluation may be needed.

Surface functionalization—Similar as other nanomaterials, the *in vivo* PK and biodistribution of CNTs are closely associated with their surface coating. Different surface coatings can significantly change the circulation half-lives of CNTs in the bloodstream, alter

their biocompatibility profile, and affect potential aggregation of individual CNT through van der Waals forces. Of note, pristine CNTs themselves are highly hydrophobic, hence not suitable for biomedical applications without surface functionalization. In order to improve hydrophilicity and water solubility, sidewall functional groups (e.g. hydroxyl and carboxyl) can be introduced onto CNTs. In addition, these functional groups can also be used to attach specific polymer coatings or biomolecules to CNTs for imaging/therapeutic purposes.

In an early report, it was found that Pluronic coating was not stable in physiological environment, which could be rapidly replaced by plasma proteins after intravenous injection [18]. This is likely the reason why a short blood circulation half-life (~1 h) was observed for CNTs in this study. Non-covalent wrapping of SWNTs with PEG grafted phospholipid (e.g. DSPE-PEG) can delay the capture of SWNTs by the MPS and lead to a prolonged circulation half-life, and longer PEG chains on the surface of SWNTs resulted in longer blood circulation half-life [31]. A subsequent report from the same group confirmed that functionalization of SWNTs with branched PEG chains can exhibit even longer circulation half-life (~5 h), which was significantly improved over SWNTs coated with linear PEG chains (a few hours) [16].

Since long blood circulation half-life is usually considered to be advantageous for nanomedicine which can offer more opportunities for enhanced tumor targeting, several strategies have been investigated to generate SWNTs with ultra-long blood circulation half-lives. In one study, covalent PEGylation of SWNTs was carried out [59]. It was reported that this strategy can increase the blood circulation half-life of SWNTs to ~22.5 h. When non-covalent PEGylation was adopted, PEG grafted poly(maleic anhydride-alt-1-octadecene) (denoted as PEG-PMHC$_{18}$) was found to exhibit remarkably long blood circulation half-life (~ 22 h) upon intravenous injection into mice [60]. Inspired by these findings, a series of amphiphilic polymers were designed by combining different lengths of PEG chains with PMHC$_{18}$ at various densities before conjugation onto SWNTs [61]. Interestingly, although ultra-long blood circulation half-life was achieved with dense PEGylation of the SWNTs, along with enhanced tumor uptake, high accumulation of these SWNTs in the mouse skin was also observed. Through controlling the degree of PEGylation on the polymer backbone, an optimal blood circulation half-life of SWNTs (~13 h) was achieved in mice with low skin accumulation [61]. It was concluded that the balance between high tumor targeting (i.e. based on long blood circulation half-life) and non-specific background uptake should be maintained. Fine-tuning the surface chemistry of SWNTs is crucial to optimize their *in vivo* PK for the desired biomedical applications.

Based on many other literature reports, specific functional groups can strongly affect the PK and fate of CNTs. For example, hydroxylated CNTs (e.g. ^{125}I-labeled SWNTs [29]) can quickly distribute throughout the whole body and accumulate in the bone for a prolonged time period, whereas taurine functionalized MWNTs that are more negatively charged predominantly accumulated in the liver for over three months with noticeable liver toxicity [37]. Intriguingly, ^{111}In-DTPA-SWNTs or MWNTs were not retained in the MPS (e.g. liver and spleen) and exhibited rapid clearance via renal excretion [26–27]. Taken together the literature findings, surface modification can significantly alter the interactions of CNTs with cellular lipid bilayer, plasma proteins, and macrophages, which can act as one determining factor for the PK and behavior of CNTs.

Morphology (length & shape)—The major morphological factor that contributes to the *in vivo* PK of CNTs is the length, since they all have similar one-dimensional shape. One study reported that macrophages can capture 220 nm-long MWNTs more readily than 825 nm-long MWNTs, and the latter triggered higher degree of inflammation [62]. Although the "cutoff" length of CNTs for macrophage capture is not known, the "shorter" CNTs (length

from 100 to 300 nm) in abovementioned studies tended to accumulate in the liver and spleen [16, 29, 31], the "medium" CNTs (length from 300 nm to 2 μm) were reported to undergo rapid renal excretion [26–27], and the "longer" CNTs (length > 2 μm) typically resulted in high uptake in the lungs along with significant retention in the liver and spleen [38, 57]. Besides the length, the shape of CNTs also matters to a certain degree. For example, long and needle-like CNTs were reported to activate IL-1 and lead to the production of a series of reactive oxygen species in macrophages [63], which can significantly affect the PK of CNTs.

Administration route—The PK and toxicity of CNTs are also strongly associated with the administration route. Although most of the current PK studies were focused on intravenous injection, other administration routes such as intraperitoneal injection [64], intratracheal administration [65], and oral gavage have also been investigated. In one study, it was found that SWNTs can coalesce with each other inside the body to form fiber-like structures after intraperitoneal administration [64], and induce granuloma formation when the structure length exceeded 10 μm. Although shorter aggregates (<300 nm) did not induce granuloma formation, they persisted inside the mouse body for up to 5 months after intraperitoneal administration. In addition, it was found that short and well-individualized SWNTs could escape the MPS to be excreted through the kidneys and bile ducts.

When CNTs were administered intratracheally into animals, an induction of inflammatory reactions in the lung was usually observed along with cardiovascular adverse effects [66–67]. However, one report also demonstrated the lack of obvious toxicity for SWNTs, which were formulated using a biocompatible nanoscale dispersion technique [68]. In this work, stable nanoscale dispersions of SWNTs were produced by ultrasonication of SWNT powder in 1 wt% aqueous solution of Pluronic F 108NF followed by ultracentrifugation, which eliminated large SWNT bundles and dense impurity species. Based on these literature reports, it is clear that surface coating is the dominant factor to determine pulmonary toxicity of CNTs *in vivo*. On the other hand, animals showed good tolerance to orally administered CNTs at doses as high as 1,000 mg/kg with no behavior abnormality [64].

PK OF QDS

Fluorescent semiconductor QDs have attracted tremendous attention over the last decade [9, 69–70]. QDs with composition and size tunable fluorescence emission have been widely used as probes for *in vitro* and *in vivo* imaging applications [71–75]. The superior optical properties of QDs over conventional organic dyes make them attractive labels for a wide variety of biomedical applications, whereas their potential toxicity and instability in biological environment has puzzled scientific researchers. In this section, we will summary the influences of surface coating (or charge), hydrodynamic (HD) size, and shape on the PK of QDs.

Effect of surface coating

Before they can be used for biological imaging studies, QDs are usually functionalized with hydrophilic polymers or molecules to increase the water solubility, and sometimes also conjugated to various ligands for specific targeting [73, 76–78]. Surface modification plays a pivotal role on the surface charge, HD size, blood circulation half-life, biodistribution, clearance, specific organ/tissue targeting, and potential degradation of QDs in living subjects.

In an early report, surface-dependent PK behavior of QDs was demonstrated [79]. It was shown that QDs with coatings such as poly(acrylic acid) (PAA), methoxy-terminated PEG of 750 Da (mPEG-750), or carboxyl-terminated PEG of 3400 Da (COOH-PEG-3400) were

all cleared from the circulation within 1 hour post-injection into mice, whereas QDs coated with mPEG-5000 exhibited a prolonged half-life of ~3 h along with significantly lower uptake in the lymph nodes and liver (Figure 4a). Similar prolonged blood half-life of QDs after suitable PEGylation was also reported for amino-PEG modified QDs [80]. It is worthy to note that QD fluorescence from lymph nodes and bone marrow could still be detected at more than four months post-injection, indicating long-term trapping, little clearance, and non-breakdown of intravenously injected QDs.

Without using any specific targeting moieties, Chio et al. demonstrated the ability to control circulation half-life, organ- and tissue-selective biodistribution, and elimination route of dihydrolipoic acid (DHLA)/PEG modified QDs (termed as QD@DHLA-PEG_n, where n = 2–22) by simply changing the length of PEG chains (Figure 4b) [81]. Interestingly, QD@DHLA-PEG_2 (HD size: 5.1 nm) accumulated primarily in the liver, while the majority of QD@DHLA-PEG_3 (HD size: 5.3 nm) ended up in the kidney and bladder. QDs with DHLA-PEG_4 coating (HD size: 5.6 nm) had accelerated body excretion via the liver and kidneys. In addition, uptake of QDs in the pancreas was only observed when QDs were coated with DHLA-PEG_8 (HD size: 6.5 nm) and DHLA-PEG_{14} (HD size: 8.7 nm). QD@DHLA-PEG_{22} (HD size: 16 nm) exhibited poor clearance and were primarily detected in the vasculature at 4 h post-injection, with delayed excretion through renal and hepatic routes when compared to the QDs coated with shorter PEG chains.

Although distribution of QDs in different organs can be visualized based on whole body fluorescence imaging, as shown in Figure 4 [79, 81], this approach is not highly accurate due to the qualitative nature of optical imaging, the prominent and variable background autofluorescence, as well as absorbance/scattering of light in blood and tissues. Furthermore, the fluorescence of QDs can be susceptible to environmental factors, which makes it even more difficult to achieve precise and quantitative evaluation of QD biodistribution [82]. In one report, the *in vivo* PK, clearance, and metabolism of CdSe@ZnS QDs (TEM size: 5.5 nm) with different surface coatings in Sprague-Dawley rats was quantitatively analyzed with inductively coupled plasma atomic emission spectroscopy (ICP-AES) [83]. When compared to QDs conjugated to bovine serum albumin (QD-BSA), QDs coated with the organic molecule mercaptoundecanoic acid and crosslinked with lysine (denoted as QD-LM) had significantly slower blood clearance. Possibly due to the larger HD diameter (~80 nm) and shorter blood circulation time ($t_{1/2}$: 38.7 ± 3.5 min), QD-BSA was found almost exclusively in the liver, with appreciable bone marrow uptake at 90 min post-injection. Both QDs exhibited similar spleen uptake of ~2% injected dose. Different from that observed in a previous report [79], only extremely low lymph node uptake was detected in this study. No detectable QDs could be found in either the feces or urine for up to 10 days post-injection, indicating minimal clearance of these QDs from the rat body.

PET imaging of small animals allows for serial imaging of live subjects, which obviates the need to sacrifice animals and minimizes inter-individual variations [23, 84–86]. In an early report, a dual-function PET/NIRF probe was constructed by labeling QD705 with ^{64}Cu, which could allow for more accurate assessment of the PK and tumor-targeting efficacy of QDs *in vivo* [87]. The amino groups on QD surface was conjugated to DOTA (for ^{64}Cu-labeling) and RGD peptides (for integrin $\alpha_v\beta_3$ targeting). Quantitative analysis of the PET data indicated liver uptake of ~50 percentage injected dose per gram (%ID/g) for both targeted and non-targeted QDs. Successful tumor targeting was achieved, since uptake of ^{64}Cu-DOTA-QD-RGD in the U87MG tumor (integrin $\alpha_v\beta_3$ positive) was significantly higher than that of ^{64}Cu-DOTA-QD at all time points examined. *Ex vivo* PET and NIRF imaging studies were also carried out to validate the *in vivo* findings. At early time points (e.g. a few hours post-injection), the results from PET (detecting ^{64}Cu) and NIRF (detecting QDs) imaging matched quite well, indicating good *in vivo* stability of the dual-function

agent. At late time points (e.g. 24 h post-injection), significant difference between PET and NIRF images could be observed, which suggested shedding of the surface polymer coating from QDs. In another study, $VEGF_{121}$ was used as the ligand for tumor vasculature targeting of QDs, and similar results were observed [88].

Using serial non-invasive small animal PET imaging, the *in vivo* fate of commercially available CdSe QDs with varied surface modifications was quantitatively investigated in nude mice [89]. Similar as that reported in previous studies [79–80], it was found that QDs with a larger HD size had a faster accumulation rate in both the liver and spleen, while PEGylated QDs exhibited slightly slower rate of accumulation in these organs. For ^{64}Cu-labeled QD800 (~21 nm in diameter) and QD525 (~12 nm), the uptake in the liver (27.4–38.9 %ID/g) and spleen (8.0–12.4 %ID/g) were similar. Bone marrow uptake was only observed for PEGylated QDs. Overall, regardless of the difference in HD size, no convincing evidence of clearance was found for either type of QDs.

Effect of size and shape

Morphology (i.e. HD size and shape) of QDs is another important parameter that can affect their PK profile *in vivo*. Many studies have suggested that the extent of non-specific binding (or adsorption) of proteins in the bloodstream is highly dependent on the nanoparticle size, curvature, hydrophobicity, surface charge, among others [90–92]. Protein adsorption on QD surface could dramatically increase the HD size, change the surface charge, and cause aggregation, thereby leading to dramatic alterations in their physicochemical properties and PK *in vivo*. Although many types of QDs cannot efficiently escape recognition and clearance by the MPS, some specially designed QDs may be able to avoid MPS sequestration and substantially extravasate in certain tumor models, which hold greater potential for more efficacious tumor targeting *in vivo* [77, 93]. Herein we will summarize the impact of HD size and shape on PK and extravasation of QDs.

Effect of HD size on biodistribution and clearance of QDs—The charge of QD surface coating has a profound effect on the adsorption of serum proteins, as well as the HD size. For example, net anionic or cationic charges are usually associated with an increase in the HD size [83]. By coating QDs with a zwitterionic surface, Choi et al. demonstrated that undesirable serum protein adsorption could be prevented to obtain a series of QDs with extremely small HD sizes [93]. Systematic *in vivo* optical and γ-camera imaging demonstrated that biodistribution and clearance of QDs is highly dependent on the HD size. It was suggested that although PEGylation could allow for delayed (or sometime negligible) MPS clearance of QDs, it increases the HD size and prevents renal excretion. Convincing evidence was provided to demonstrate that only QDs with a final HD size below 5.5 nm could be excreted through the urine [93]. In a follow-up study, these researchers further demonstrated *in vivo* active targeting and renal clearance of RGD peptide-conjugated QDs within 4 h post-injection [77]. Since potential toxicity and slow clearance are two major obstacles for clinical translation of QDs, especially the long-term effect and unpredictable hepatic clearance, these two studies provided a foundation for the design and development of molecularly targeted imaging agents for future cancer diagnosis and therapy with QDs and other nanoparticles [77, 93].

Subsequently, many studies have further confirmed that QDs with HD sizes larger than the renal clearance cutoff (~5.5 nm) usually ended up in the liver and spleen, with only very limited clearance over the study period [94–95]. Although QDs have been reported to maintain their fluorescence signal over months or even years in animals [79, 94], the degradation of surface coating and potential breakdown of QDs *in vivo* are still under debate. In an *in vitro* study, it was suggested that surface coating of QDs may not be as

stable as previously imagined [96]. Appropriate choice of both nanoparticle size and monolayer structure was considered to be critical for future imaging applications.

In fact, several long-term toxicity studies did suggest the degradation of QDs *in vivo*. In a recently reported pilot toxicity study in rhesus macaques by intravenous injection of 25 mg/kg of phospholipid micelle encapsulated CdSe@CdS@ZnS QDs (~52 nm), a surprisingly higher Cd-to-Se ratio in the kidney was observed based on the ICP-MS results, when compared with that of the liver and spleen at day 90 post-injection (Figure 5) [97]. Since no QD fluorescence signal could be detected in the kidney despite the high concentration of elemental constituents of QDs, the break-down or slow degradation of QDs may be the only reasonable explanation for the different Cd-to-Se ratio in different organs. Although many previous reports have demonstrated that degradation of surface coating *in vivo* could compromise the stability/utility of QDs and result in potential toxicity *in vivo* [98–99], surprisingly, no clear evidence of toxicity was observed within three months in this study [97]. Blood and biochemical markers remained within normal ranges, and histology of major organs showed no abnormalities. ICP-MS analysis further revealed dominant Cd element distribution in the liver (~58 %ID), spleen (~6 %ID), and kidney (~35 %ID) at day 90 post-injection. Importantly, > 90% of injected Cd remained in the animals after 90 days. In a previous study carried out in rats, QDs were also found to be sequestered with no excretion based on measurement of Cd element in the bile, intestinal lumen, and kidney [100].

Similar and more obvious redistribution of QDs from liver to kidneys has been observed in other studies [101–102]. For example, the biodistribution of aqueous QDs with HD sizes ranging from 2.9 to 4.5 nm were investigated [101]. A rapid accumulation of QDs in the liver (up to 30 %ID/g) was observed over a short-term, followed by increased accumulation in the kidneys (40 %ID/g) after 80 days. QDs of larger HD size were demonstrated to have a quicker accumulation in the spleen. No overt toxicity of QDs after 80 days of exposure was detected, based on histological and biochemical analyses.

Effect of size and shape on extravasation—In a series of studies, we have shown that RGD peptide conjugated NIRF QDs could be specifically targeted to U87MG human glioblastoma tumors *in vivo*, which express high levels of integrin $\alpha_v\beta_3$ on both the tumor cells and the tumor vasculature [78, 87, 103]. Immunofluorescence staining confirmed specific integrin $\alpha_v\beta_3$ targeting of these QDs to the tumor vasculature, and the vast majority of injected RGD conjugated QDs did not extravasate (far) from the tumor vessels. A series of subsequent studies further demonstrated that extravasation of QDs is highly complex, which may depend on many factors including the size and shape of QDs, surface modifications, tumor types, among others [104–106].

Different behaviors in extravasation from the normal vasculature to interstitial fluid were investigated in rat models, using DHLA coated and DHLA-PEG coated InAs@ZnSe QDs [107]. Obvious extravasation of QD@DHLA-PEG (HD size: 8.7 nm) was observed based on NIRF imaging, whereas minimal extravasation was found for QD@DHLA (HD size: 13.8 nm). Although both QDs were reported to have similar circulation half-lives, it was suggested that the increased HD size of QD@DHLA (from 5.3 nm in phosphate-buffered saline to 13.8 nm in fetal bovine serum) caused by non-specific protein binding *in vitro*/*in vivo* could be the main reason behind such differences.

Using intravital microscopy which has subcellular resolution, the real-time specific binding of RGD conjugated QDs to integrin $\alpha_v\beta_3$ on tumor neovasculature was studied in mouse tumor models [105–106]. Intriguingly, it was found that the binding rates and binding patterns between various tumor types did not vary significantly. However, striking

difference was observed with regard to extravasation of QDs from tumor vasculature. Little extravasation of RGD conjugated QDs (HD size: 5–25 nm) was observed in xenograft SKOV-3 ovarian cancer and U87MG glioblastoma models in nude mice. On the other hand, unequivocal and rapid extravasation of QDs from blood vessels in xenograft LS174T colorectal tumors was found in mice injected with similar doses of the same QD conjugates. Clearly, HD size is not the only factor that governs QD extravasation in tumors. The heterogeneity of tumor neovasculature across different tumor types also plays a significant role.

In a follow-up study, these investigators extended their research to study and quantify the differences in extravasation of QDs (HD size: 20–25 nm) and SWNTs (~200 nm in length), the two commonly used but very differently shaped nanoparticles [104]. Both nanoparticles were designed to possess similar charge, surface coating, and density. Different from the clear extravasation that was observed in an abovementioned report [107], no extravasation of either QDs or SWNTs from normal vasculature was found in mice implanted with any of the three tumor types (U87MG, LS174T, and SKOV-3) [104]. Detailed investigation revealed that neither nanoparticle extravasated in the SKOV-3 tumors, which was suggested to be due to the small pore size cutoff of the vasculature. In the LS174T and U87MG tumors, the extent and dynamics of extravasation was reported to be highly complex: significantly more extravasation was detected for QDs than SWNTs in the LS174T tumor, where the opposite was observed in the U87MG tumor (Figure 6). *In vitro* simulated diffusion experiments were carried out to provide a rationale for such findings. However, the exact reason behind such surprising geometrical dependence of nanoparticles in tumor extravasation remain to be elucidated in future studies.

CONCLUSION AND FUTURE PERSPECTIVES

Molecular imaging is one of the most vibrant areas of research over the last decade, not only in oncology but also in many other disciplines [5, 108–110]. A wide variety of nanoparticles have been investigated for imaging and therapeutic applications, which spanned every single imaging modality [8]. With the rapid development of nanotechnology, humans may be exposed to various nanoparticles through inhalation, ingestion, skin contact and uptake, intravenous injection, etc. The long-term impact of many nanoparticles is poorly understood to date, and conflicting results have often been reported, partly due to the fact that the PK and biodistribution of nanoparticles is dependent upon multiple factors such as size, shape, surface charge, surface chemistry, and many others. Through rational design and optimization of these factors, non-specific uptake of nanoparticles can be greatly reduced and blood circulation can be prolonged, thereby conferring the nanoparticles enhanced opportunities to home to the targeted tissue (e.g. tumor, cardiovascular diseases, etc.).

Various imaging techniques have been employed to evaluate the PK of nanoparticles, among which radionuclide-based imaging (especially PET) can provide the highest detection sensitivity (down to picomolar level) and offer high clinical relevance. However, despite the many strategies that have been explored to increase the overall stability of conjugated nanoparticles and prevent the radioisotopes from dissociation [30, 38], potential detachment of radioisotopes from the nanoparticles remains a major concern which can significantly complicate the interpretation of experimental findings. Rigorous validation of the *in vivo* findings with *ex vivo* measurements are always needed to provide more reliable results. To obtain more accurate PK profile, imaging techniques that can capture the intrinsic physical or chemical signals from the nanoparticle itself may be more desirable. For example, the intense Raman signal from SWNTs [16, 64, 111] and the strong and stable fluorescence signal from QDs [75, 93] can be good candidates for PK investigation, with the caveat that both Raman and fluorescence imaging suffer from poor signal penetration in tissues, hence

only suitable for small animal studies. MRI was also used for PK studies of nanoparticles. However, the inherent low sensitivity severely limits the utility of this imaging technique for *in vivo* PK assessment. With regard to PK evaluation of SWNTs, in some cases MRI detects the metal doping or the effect triggered by metal impurities from SWNTs rather than the SWNTs themselves [19, 56], which is suboptimal and can complicate the scenarios.

Based on the available literature reports on PK studies of QDs and SWNTs, a few general principles can be established. First, surface functionalization is the most important factor to alter and fine-tune the PK of nanoparticles. Let's take CNTs as the example: optimally surface-functionalized CNTs with biocompatible coating (e.g. PEGylation) exhibited much lower toxicity, prolonged blood circulation half-life, reduced uptake in the MPS, and enhanced tumor-targeting efficiency *in vivo* than the CNTs without appropriate surface coating. The same rule is also generally applicable for QD-based agents. Second, besides the surface functionalization/chemistry, morphology of nanoparticles also matters. The right shape and size of nanoparticles can result in less non-specific capture by macrophages, which can also affect their excretion route, circulation half-life, as well as how they will interact with different tissues *in vivo*. Last but not least, the route from which the nanoparticles enter the body and the dose administered also contributes to the overall PK profile of nanoparticles. Oral administration of nanoparticles can be well-tolerated at a comparatively high dose, while intravenous/intraperitoneal/intratracheal administration of nanoparticles may be more likely to trigger acute and/or chronic toxicity, which can be closely associated with their surface chemistry.

Recently, nanotoxicology has emerged as a new branch of toxicology for studying the undesirable effects of nanoparticles [112–115]. Development of novel nanoparticles for biomedical applications must proceed in tandem with the assessment of any toxicological side effects. A thorough understanding of the PK profiles of various nanoparticles is necessary for risk assessment and minimizing any adverse effects to the patients or the environment. We believe that the key question is not how toxic the nanoparticles themselves are, but how to modify and functionalize them so that they do not exhibit acute/chronic toxicity, can be cleared from the body over time, and thereby can be best used for biomedical applications. Robust chemistry for surface modification of nanoparticles is the key to success in future biomedical and clinical applications.

It is anticipated that the emergence of new nanotechnology will facilitate the development of novel drug delivery systems that can not only specifically deliver a drug to the target tissue, but also release it locally and efficiently. The future of nanomedicine lies in multifunctional nanoplatforms which combine both therapeutic components and non-invasive imaging. Such integration of diagnostic imaging capability with therapeutic interventions, often termed as "theranostics" [14, 116–118], is critical to addressing the challenges of cancer heterogeneity and adaptation. With the unprecedented initiatives such as the NCI Alliance for Nanotechnology in Cancer that encompasses the public and private sectors, designed to accelerate the applications of the best capabilities of nanotechnology to cancer [2], it is expected that promising molecular discoveries will be efficiently translated into the clinic to benefit (cancer) patients. Nanotechnology can provide the technical power and tools that will enable the development of new diagnostics, therapeutics, and preventives which can radically change the way we diagnose, treat, and prevent cancer.

Acknowledgments

This work is supported, in part, by the University of Wisconsin Carbone Cancer Center, the National Institutes of Health (1R01CA169365 - 01A1), the Department of Defense (W81XWH-11-1-0644), UW Graduate School, and UW Department of Radiology.

References

1. Ferrari M. Cancer nanotechnology: opportunities and challenges. Nat Rev Cancer. 2005; 5:161–171. [PubMed: 15738981]
2. Farrell D, Alper J, Ptak K, et al. Recent advances from the National Cancer Institute Alliance for Nanotechnology in Cancer. ACS Nano. 2010; 4:589–594. [PubMed: 20175564]
3. Hong H, Zhang Y, Sun J, Cai W. Molecular imaging and therapy of cancer with radiolabeled nanoparticles. Nano Today. 2009; 4:399–413. [PubMed: 20161038]
4. Li SD, Huang L. Pharmacokinetics and biodistribution of nanoparticles. Mol Pharm. 2008; 5:496–504. [PubMed: 18611037]
5. James ML, Gambhir SS. A molecular imaging primer: modalities, imaging agents, and applications. Physiol Rev. 2012; 92:897–965. [PubMed: 22535898]
6. Mankoff DA. A definition of molecular imaging. J Nucl Med. 2007; 48:18N, 21N.
7. Nolting DD, Nickels ML, Guo N, Pham W. Molecular imaging probe development: a chemistry perspective. Am J Nucl Med Mol Imaging. 2012; 2:273–306. [PubMed: 22943038]
8. Cai W, Chen X. Nanoplatforms for targeted molecular imaging in living subjects. Small. 2007; 3:1840–1854. [PubMed: 17943716]
9. Cai W, Hsu AR, Li ZB, Chen X. Are quantum dots ready for *in vivo* imaging in human subjects? Nanoscale Res Lett. 2007; 2:265–281. [PubMed: 21394238]
10. Yigit MV, Medarova Z. *In vivo* and *ex vivo* applications of gold nanoparticles for biomedical SERS imaging. Am J Nucl Med Mol Imaging. 2012; 2:232–241. [PubMed: 23133814]
11. Hong H, Gao T, Cai W. Molecular Imaging with Single-Walled Carbon Nanotubes. Nano Today. 2009; 4:252–261. [PubMed: 21754949]
12. Liu Z, Tabakman S, Welsher K, Dai H. Carbon Nanotubes in Biology and Medicine: *In vitro* and *in vivo* Detection, Imaging and Drug Delivery. Nano Res. 2009; 2:85–120. [PubMed: 20174481]
13. Yang K, Liu Z. *In vivo* biodistribution, pharmacokinetics, and toxicology of carbon nanotubes. Curr Drug Metab. 2012; 13:1057–1067. [PubMed: 22380009]
14. Liu Z, Liang XJ. Nano-carbons as theranostics. Theranostics. 2012; 2:235–237. [PubMed: 22448193]
15. Lacerda L, Bianco A, Prato M, Kostarelos K. Carbon nanotubes as nanomedicines: from toxicology to pharmacology. Adv Drug Deliv Rev. 2006; 58:1460–1470. [PubMed: 17113677]
16. Liu Z, Davis C, Cai W, et al. Circulation and long-term fate of functionalized, biocompatible single-walled carbon nanotubes in mice probed by Raman spectroscopy. Proc Natl Acad Sci USA. 2008; 105:1410–1415. [PubMed: 18230737]
17. Schipper ML, Nakayama-Ratchford N, Davis CR, et al. A pilot toxicology study of single-walled carbon nanotubes in a small sample of mice. Nat Nanotechnol. 2008; 3:216–221. [PubMed: 18654506]
18. Cherukuri P, Gannon CJ, Leeuw TK, et al. Mammalian pharmacokinetics of carbon nanotubes using intrinsic near-infrared fluorescence. Proc Natl Acad Sci USA. 2006; 103:18882–18886. [PubMed: 17135351]
19. Al Faraj A, Fauvelle F, Luciani N, et al. *In vivo* biodistribution and biological impact of injected carbon nanotubes using magnetic resonance techniques. Int J Nanomedicine. 2011; 6:351–361. [PubMed: 21499425]
20. Bai Y, Zhang Y, Zhang J, et al. Repeated administrations of carbon nanotubes in male mice cause reversible testis damage without affecting fertility. Nat Nanotechnol. 2010; 5:683–689. [PubMed: 20693989]
21. Gambhir SS. Molecular imaging of cancer with positron emission tomography. Nat Rev Cancer. 2002; 2:683–693. [PubMed: 12209157]
22. Gambhir SS, Czernin J, Schwimmer J, et al. A tabulated summary of the FDG PET literature. J Nucl Med. 2001; 42:1S–93S. [PubMed: 11483694]
23. Alauddin MM. Positron emission tomography (PET) imaging with ^{18}F-based radiotracers. Am J Nucl Med Mol Imaging. 2012; 2:55–76. [PubMed: 23133802]

24. Fakhri GE. Ready for prime time? Dual tracer PET and SPECT imaging. Am J Nucl Med Mol Imaging. 2012; 2:415–417. [PubMed: 23145358]
25. Bhargava P, He G, Samarghandi A, Delpassand ES. Pictorial review of SPECT/CT imaging applications in clinical nuclear medicine. Am J Nucl Med Mol Imaging. 2012; 2:221–231. [PubMed: 23133813]
26. Lacerda L, Soundararajan A, Singh R, et al. Dynamic Imaging of Functionalized Multi-Walled Carbon Nanotube Systemic Circulation and Urinary Excretion. Adv Mater. 2008; 20:225–230.
27. Singh R, Pantarotto D, Lacerda L, et al. Tissue biodistribution and blood clearance rates of intravenously administered carbon nanotube radiotracers. Proc Natl Acad Sci USA. 2006; 103:3357–3362. [PubMed: 16492781]
28. McDevitt MR, Chattopadhyay D, Kappel BJ, et al. Tumor targeting with antibody-functionalized, radiolabeled carbon nanotubes. J Nucl Med. 2007; 48:1180–1189. [PubMed: 17607040]
29. Wang H, Wang J, Deng X, et al. Biodistribution of carbon single-wall carbon nanotubes in mice. J Nanosci Nanotechnol. 2004; 4:1019–1024. [PubMed: 15656196]
30. Hong SY, Tobias G, Al-Jamal KT, et al. Filled and glycosylated carbon nanotubes for *in vivo* radioemitter localization and imaging. Nat Mater. 2010; 9:485–490. [PubMed: 20473287]
31. Liu Z, Cai W, He L, et al. *In vivo* biodistribution and highly efficient tumour targeting of carbon nanotubes in mice. Nat Nanotechnol. 2007; 2:47–52. [PubMed: 18654207]
32. Cai W, Niu G, Chen X. Imaging of integrins as biomarkers for tumor angiogenesis. Curr Pharm Des. 2008; 14:2943–2973. [PubMed: 18991712]
33. McDevitt MR, Chattopadhyay D, Jaggi JS, et al. PET imaging of soluble yttrium-86-labeled carbon nanotubes in mice. PLoS One. 2007; 2:e907. [PubMed: 17878942]
34. Zhang Y, Hong H, Cai W. PET tracers based on Zirconium-89. Curr Radiopharm. 2011; 4:131–139. [PubMed: 22191652]
35. van Dongen GA, Ussi AE, de Man FH, Migliaccio G. EATRIS, a European initiative to boost translational biomedical research. Am J Nucl Med Mol Imaging. 2013; 3:166–174. [PubMed: 23526583]
36. Ruggiero A, Villa CH, Holland JP, et al. Imaging and treating tumor vasculature with targeted radiolabeled carbon nanotubes. Int J Nanomedicine. 2010; 5:783–802. [PubMed: 21042424]
37. Deng X, Jia G, Wang H, et al. Translocation and fate of multi-walled carbon nanotubes *in vivo*. Carbon. 2007; 45:1419–1424.
38. Georgin D, Czarny B, Botquin M, et al. Preparation of ^{14}C-labeled multiwalled carbon nanotubes for biodistribution investigations. J Am Chem Soc. 2009; 131:14658–14659. [PubMed: 19788249]
39. Zhang Y, Hong H, Myklejord DV, Cai W. Molecular imaging with SERS-active nanoparticles. Small. 2011; 7:3261–3269. [PubMed: 21932216]
40. Jorio A, Saito R, Dresselhaus G, Dresselhaus MS. Determination of nanotubes properties by Raman spectroscopy. Philos Transact A Math Phys Eng Sci. 2004; 362:2311–2336.
41. Keren S, Zavaleta C, Cheng Z, et al. Noninvasive molecular imaging of small living subjects using Raman spectroscopy. Proc Natl Acad Sci USA. 2008; 105:5844–5849. [PubMed: 18378895]
42. Zavaleta C, de la Zerda A, Liu Z, et al. Noninvasive Raman spectroscopy in living mice for evaluation of tumor targeting with carbon nanotubes. Nano Lett. 2008; 8:2800–2805. [PubMed: 18683988]
43. Cai W, Hong H. In a “nutshell”: intrinsically radio-labeled quantum dots. Am J Nucl Med Mol Imaging. 2012; 2:136–140. [PubMed: 23133808]
44. Thorek D, Robertson R, Bacchus WA, et al. Cerenkov imaging - a new modality for molecular imaging. Am J Nucl Med Mol Imaging. 2012; 2:163–173. [PubMed: 23133811]
45. Wu Y, Zhang W, Li J, Zhang Y. Optical imaging of tumor microenvironment. Am J Nucl Med Mol Imaging. 2013; 3:1–15. [PubMed: 23342297]
46. Kim C, Favazza C, Wang LV. *In vivo* photoacoustic tomography of chemicals: high-resolution functional and molecular optical imaging at new depths. Chem Rev. 2010; 110:2756–2782. [PubMed: 20210338]
47. Wang LV, Hu S. Photoacoustic tomography: *in vivo* imaging from organelles to organs. Science. 2012; 335:1458–1462. [PubMed: 22442475]

48. Wang LV. Prospects of photoacoustic tomography. Med Phys. 2008; 35:5758–5767. [PubMed: 19175133]
49. De la Zerda A, Zavaleta C, Keren S, et al. Carbon nanotubes as photoacoustic molecular imaging agents in living mice. Nat Nanotechnol. 2008; 3:557–562. [PubMed: 18772918]
50. de la Zerda A, Liu Z, Bodapati S, et al. Ultrahigh sensitivity carbon nanotube agents for photoacoustic molecular imaging in living mice. Nano Lett. 2010; 10:2168–2172. [PubMed: 20499887]
51. Avti PK, Hu S, Favazza C, et al. Detection, mapping, and quantification of single walled carbon nanotubes in histological specimens with photoacoustic microscopy. PLoS One. 2012; 7:e35064. [PubMed: 22496892]
52. Sosnovik DE, Weissleder R. Emerging concepts in molecular MRI. Curr Opin Biotechnol. 2007; 18:4–10. [PubMed: 17126545]
53. Weissleder R, Pittet MJ. Imaging in the era of molecular oncology. Nature. 2008; 452:580–589. [PubMed: 18385732]
54. Sitharaman B, Kissell KR, Hartman KB, et al. Superparamagnetic gadonanotubes are high-performance MRI contrast agents. Chem Commun (Camb). 2005:3915–3917. [PubMed: 16075070]
55. van der Zande M, Sitharaman B, Walboomers XF, et al. *In Vivo* Magnetic Resonance Imaging of the Distribution Pattern of Gadonanotubes Released from a Degrading Poly(Lactic-Co-Glycolic Acid) Scaffold. Tissue Eng Part C Methods. 2011; 17:19–26.
56. Al Faraj A, Cieslar K, Lacroix G, et al. *In vivo* imaging of carbon nanotube biodistribution using magnetic resonance imaging. Nano Lett. 2009; 9:1023–1027. [PubMed: 19199447]
57. Yang, S-t; Guo, W.; Lin, Y., et al. Biodistribution of Pristine Single-Walled Carbon Nanotubes *In Vivo*. J Phys Chem C. 2007; 111:17761–17764.
58. Tucker-Schwartz JM, Hong T, Colvin DC, et al. Dual-modality photothermal optical coherence tomography and magnetic-resonance imaging of carbon nanotubes. Opt Lett. 2012; 37:872–874. [PubMed: 22378422]
59. Yang S-T, Fernando KAS, Liu J-H, et al. Covalently PEGylated Carbon Nanotubes with Stealth Character *In Vivo*. Small. 2008; 4:940–944. [PubMed: 18574799]
60. Prencipe G, Tabakman SM, Welsher K, et al. PEG Branched Polymer for Functionalization of Nanomaterials with Ultralong Blood Circulation. J Am Chem Soc. 2009; 131:4783–4787. [PubMed: 19173646]
61. Liu X, Tao H, Yang K, et al. Optimization of surface chemistry on single-walled carbon nanotubes for *in vivo* photothermal ablation of tumors. Biomaterials. 2011; 32:144–151. [PubMed: 20888630]
62. Sato Y, Yokoyama A, Shibata K, et al. Influence of length on cytotoxicity of multi-walled carbon nanotubes against human acute monocytic leukemia cell line THP-1 *in vitro* and subcutaneous tissue of rats *in vivo*. Mol Biosyst. 2005; 1:176–182. [PubMed: 16880981]
63. Palomaki J, Valimaki E, Sund J, et al. Long, needle-like carbon nanotubes and asbestos activate the NLRP3 inflammasome through a similar mechanism. ACS Nano. 2011; 5:6861–6870. [PubMed: 21800904]
64. Kolosnjaj-Tabi J, Hartman KB, Boudjemaa S, et al. *In vivo* behavior of large doses of ultrashort and full-length single-walled carbon nanotubes after oral and intraperitoneal administration to Swiss mice. ACS Nano. 2010; 4:1481–1492. [PubMed: 20175510]
65. Li Z, Hulderman T, Salmen R, et al. Cardiovascular effects of pulmonary exposure to single-wall carbon nanotubes. Environ Health Perspect. 2007; 115:377–382. [PubMed: 17431486]
66. Crouzier D, Follot S, Gentilhomme E, et al. Carbon nanotubes induce inflammation but decrease the production of reactive oxygen species in lung. Toxicology. 2010; 272:39–45. [PubMed: 20381574]
67. Warheit DB, Laurence BR, Reed KL, et al. Comparative pulmonary toxicity assessment of single-wall carbon nanotubes in rats. Toxicol Sci. 2004; 77:117–125. [PubMed: 14514968]
68. Mutlu GM, Budinger GR, Green AA, et al. Biocompatible nanoscale dispersion of single-walled carbon nanotubes minimizes *in vivo* pulmonary toxicity. Nano Lett. 2010; 10:1664–1670. [PubMed: 20377197]

69. Michalet X, Pinaud FF, Bentolila LA, et al. Quantum dots for live cells, *in vivo* imaging, and diagnostics. Science. 2005; 307:538–544. [PubMed: 15681376]
70. Sun M, Hoffman D, Sundaresan G, Yang L, et al. Synthesis and characterization of intrinsically radiolabeled quantum dots for bimodal detection. Am J Nucl Med Mol Imaging. 2012; 2:122–135. [PubMed: 23133807]
71. Peng XG, Manna L, Yang WD, et al. Shape control of CdSe nanocrystals. Nature. 2000; 404:59–61. [PubMed: 10716439]
72. Jaiswal JK, Mattoussi H, Mauro JM, Simon SM. Long-term multiple color imaging of live cells using quantum dot bioconjugates. Nat Biotechnol. 2003; 21:47–51. [PubMed: 12459736]
73. Gao X, Cui Y, Levenson RM, Chung LW, Nie S. *In vivo* cancer targeting and imaging with semiconductor quantum dots. Nat Biotechnol. 2004; 22:969–976. [PubMed: 15258594]
74. Jaiswal JK, Goldman ER, Mattoussi H, Simon SM. Use of quantum dots for live cell imaging. Nat Methods. 2004; 1:73–78. [PubMed: 16138413]
75. Kim S, Lim YT, Soltesz EG, et al. Near-infrared fluorescent type II quantum dots for sentinel lymph node mapping. Nat Biotechnol. 2004; 22:93–97. [PubMed: 14661026]
76. Medintz IL, Uyeda HT, Goldman ER, Mattoussi H. Quantum dot bioconjugates for imaging, labelling and sensing. Nat Mater. 2005; 4:435–446. [PubMed: 15928695]
77. Choi HS, Liu W, Liu F, et al. Design considerations for tumour-targeted nanoparticles. Nat Nanotechnol. 2010; 5:42–47. [PubMed: 19893516]
78. Cai W, Shin DW, Chen K, et al. Peptide-labeled near-infrared quantum dots for imaging tumor vasculature in living subjects. Nano Lett. 2006; 6:669–676. [PubMed: 16608262]
79. Ballou B, Lagerholm BC, Ernst LA, et al. Noninvasive imaging of quantum dots in mice. Bioconjug Chem. 2004; 15:79–86. [PubMed: 14733586]
80. Daou TJ, Li L, Reiss P, Josserand V, Texier I. Effect of poly(ethylene glycol) length on the *in vivo* behavior of coated quantum dots. Langmuir. 2009; 25:3040–3044. [PubMed: 19437711]
81. Choi HS, Ipe BI, Misra P, et al. Tissue- and organ-selective biodistribution of NIR fluorescent quantum dots. Nano Lett. 2009; 9:2354–2359. [PubMed: 19422261]
82. Li CL, Murase N. Surfactant-dependent photoluminescence of CdTe nanocrystals in aqueous solution. Chem Lett. 2005; 34:92–93.
83. Fischer HC, Liu LC, Pang KS, Chan WCW. Pharmacokinetics of nanoscale quantum dots: *In vivo* distribution, sequestration, and clearance in the rat. Adv Funct Mater. 2006; 16:1299–1305.
84. Pomper MG, Lee JS. Small animal imaging in drug development. Curr Pharm Des. 2005; 11:3247–3272. [PubMed: 16250853]
85. Liu S, Park R, Conti PS, Li Z. “Kit like” (18)F labeling method for synthesis of RGD peptide-based PET probes. Am J Nucl Med Mol Imaging. 2013; 3:97–101. [PubMed: 23342304]
86. Zhang Y, Hong H, Engle JW, et al. Positron Emission Tomography and Near-Infrared Fluorescence Imaging of Vascular Endothelial Growth Factor with Dual-Labeled Bevacizumab. Am J Nucl Med Mol Imaging. 2012; 2:1–13. [PubMed: 22229128]
87. Cai W, Chen K, Li ZB, et al. Dual-function probe for PET and near-infrared fluorescence imaging of tumor vasculature. J Nucl Med. 2007; 48:1862–1870. [PubMed: 17942800]
88. Chen K, Li ZB, Wang H, et al. Dual-modality optical and positron emission tomography imaging of vascular endothelial growth factor receptor on tumor vasculature using quantum dots. Eur J Nucl Med Mol Imaging. 2008; 35:2235–2244. [PubMed: 18566815]
89. Schipper ML, Cheng Z, Lee SW, et al. microPET-based biodistribution of quantum dots in living mice. J Nucl Med. 2007; 48:1511–1518. [PubMed: 17704240]
90. Lacerda SH, Park JJ, Meuse C, et al. Interaction of gold nanoparticles with common human blood proteins. ACS Nano. 2010; 4:365–379. [PubMed: 20020753]
91. Karmali PP, Simberg D. Interactions of nanoparticles with plasma proteins: implication on clearance and toxicity of drug delivery systems. Expert Opin Drug Deliv. 2011; 8:343–357. [PubMed: 21291354]
92. Choi HS, Gibbs SL, Lee JH, et al. Targeted zwitterionic near-infrared fluorophores for improved optical imaging. Nat Biotechnol. 2013; 31:148–153. [PubMed: 23292608]

93. Choi HS, Liu W, Misra P, et al. Renal clearance of quantum dots. Nat Biotechnol. 2007; 25:1165–1170. [PubMed: 17891134]

94. Fitzpatrick JA, Andreko SK, Ernst LA, et al. Long-term persistence and spectral blue shifting of quantum dots *in vivo*. Nano Lett. 2009; 9:2736–2741. [PubMed: 19518087]

95. Yong K-T, Roy I, Ding H, et al. Biocompatible Near-Infrared Quantum Dots as Ultrasensitive Probes for Long-Term *in vivo* Imaging Applications. Small. 2009; 5:1997–2004. [PubMed: 19466710]

96. Zhu ZJ, Yeh YC, Tang R, et al. Stability of quantum dots in live cells. Nat Chem. 2011; 3:963–968. [PubMed: 22109277]

97. Ye L, Yong KT, Liu LW, et al. A pilot study in non-human primates shows no adverse response to intravenous injection of quantum dots. Nat Nanotechnol. 2012; 7:453–458. [PubMed: 22609691]

98. Derfus AM, Chan WCW, Bhatia SN. Probing the cytotoxicity of semiconductor quantum dots. Nano Lett. 2004; 4:11–18.

99. Kirchner C, Liedl T, Kudera S, et al. Cytotoxicity of colloidal CdSe and CdSe/ZnS nanoparticles. Nano Lett. 2005; 5:331–338. [PubMed: 15794621]

100. Fischer HC, Liu LC, Pang KS, Chan WCW. Pharmacokinetics of nanoscale quantum dots: *In vivo* distribution, sequestration, and clearance in the rat. Adv Funct Mater. 2006; 16:1299–1305.

101. Yang RS, Chang LW, Wu JP, et al. Persistent tissue kinetics and redistribution of nanoparticles, quantum dot 705, in mice: ICP-MS quantitative assessment. Environ Health Perspect. 2007; 115:1339–1343. [PubMed: 17805425]

102. Su Y, Peng F, Jiang Z, et al. *In vivo* distribution, pharmacokinetics, and toxicity of aqueous synthesized cadmium-containing quantum dots. Biomaterials. 2011; 32:5855–5862. [PubMed: 21601920]

103. Cai W, Chen X. Preparation of peptide conjugated quantum dots for tumour vasculature targeted imaging. Nat Protoc. 2008; 3:89–96. [PubMed: 18193025]

104. Smith BR, Kempen P, Bouley D, et al. Shape matters: intravital microscopy reveals surprising geometrical dependence for nanoparticles in tumor models of extravasation. Nano Lett. 2012; 12:3369–3377. [PubMed: 22650417]

105. Smith BR, Cheng Z, De A, et al. Real-time intravital imaging of RGD-quantum dot binding to luminal endothelium in mouse tumor neovasculature. Nano Lett. 2008; 8:2599–2606. [PubMed: 18386933]

106. Smith BR, Cheng Z, De A, et al. Dynamic Visualization of RGD-Quantum Dot Binding to Tumor Neovasculature and Extravasation in Multiple Living Mouse Models Using Intravital Microscopy. Small. 2010; 6:2222–2229. [PubMed: 20862677]

107. Zimmer JP, Kim SW, Ohnishi S, et al. Size series of small indium arsenide-zinc selenide core-shell nanocrystals and their application to *in vivo* imaging. J Am Chem Soc. 2006; 128:2526–2527. [PubMed: 16492023]

108. Temma T, Saji H. Radiolabelled probes for imaging of atherosclerotic plaques. Am J Nucl Med Mol Imaging. 2012; 2:432–447. [PubMed: 23145360]

109. Zeman MN, Scott PJ. Current imaging strategies in rheumatoid arthritis. Am J Nucl Med Mol Imaging. 2012; 2:174–220. [PubMed: 23133812]

110. Zhang L, Chang RC, Chu LW, Mak HK. Current neuroimaging techniques in Alzheimer's disease and applications in animal models. Am J Nucl Med Mol Imaging. 2012; 2:386–404. [PubMed: 23133824]

111. Choi JH, Nguyen FT, Barone PW, et al. Multimodal biomedical imaging with asymmetric single-walled carbon nanotube/iron oxide nanoparticle complexes. Nano Lett. 2007; 7:861–867. [PubMed: 17335265]

112. Krug HF, Wick P. Nanotoxicology: an interdisciplinary challenge. Angew Chem Int Ed Engl. 2011; 50:1260–1278. [PubMed: 21290492]

113. Boczkowski J, Hoet P. What's new in nanotoxicology? Implications for public health from a brief review of the 2008 literature. Nanotoxicology. 2010; 4:1–14. [PubMed: 20795899]

114. Crist RM, Grossman JH, Patri AK, et al. Common pitfalls in nanotechnology: lessons learned from NCI's Nanotechnology Characterization Laboratory. Integr Biol (Camb). 2013; 5:66–73. [PubMed: 22772974]

115. Stern ST, McNeil SE. Nanotechnology safety concerns revisited. Toxicol Sci. 2008; 101:4–21. [PubMed: 17602205]

116. Ding H, Wu F. Image guided biodistribution and pharmacokinetic studies of theranostics. Theranostics. 2012; 2:1040–1053. [PubMed: 23227121]

117. Ho YP, Leong KW. Quantum dot-based theranostics. Nanoscale. 2010; 2:60–68. [PubMed: 20648364]

118. Swierczewska M, Lee S, Chen X. Moving theranostics trom bench to bedside in an interdisciplinary research team. Ther Deliv. 2011; 2:165–170. [PubMed: 22833942]

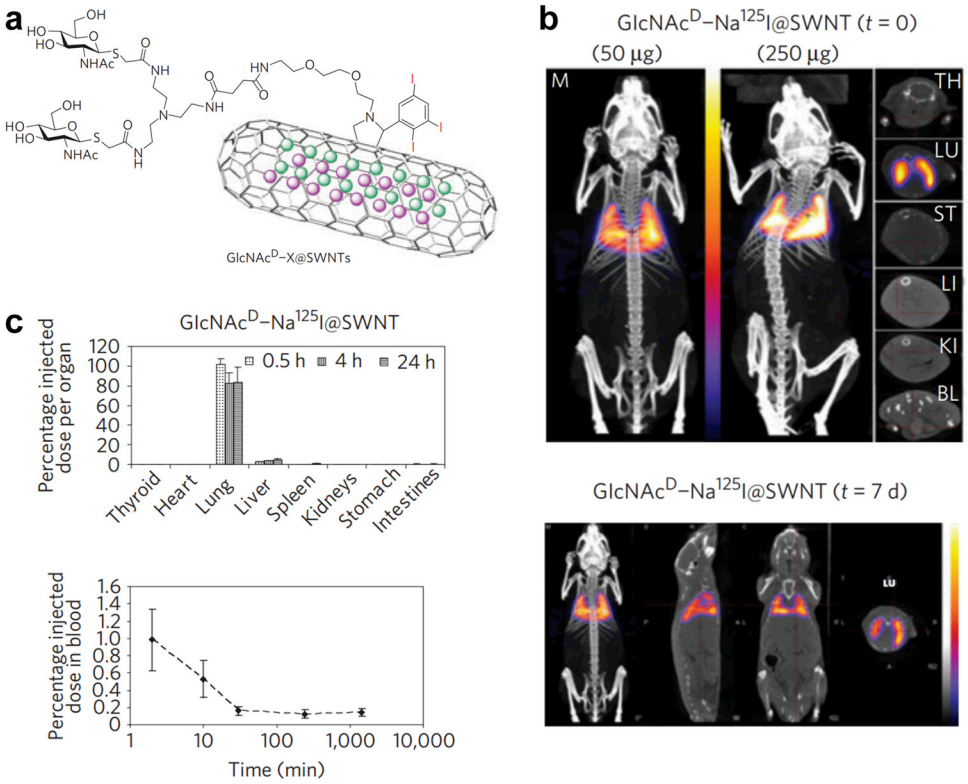

Fig. 1.

a The structure of ^{125}I-encapsulated, carbohydrate-modified SWNTs. **b** SPECT/CT images acquired immediately and 7 days after injection of GlcNAc^{D}-Na^{125}I@SWNTs. Cross-sections of the thyroid (TH), lung (LU), stomach (ST), liver (LI), kidney (KI) and bladder (BL) are also shown. **c** Tissue biodistribution and blood clearance profile of GlcNAc^{D}-Na^{125}I@SWNTs. Adapted with permission from reference [30].

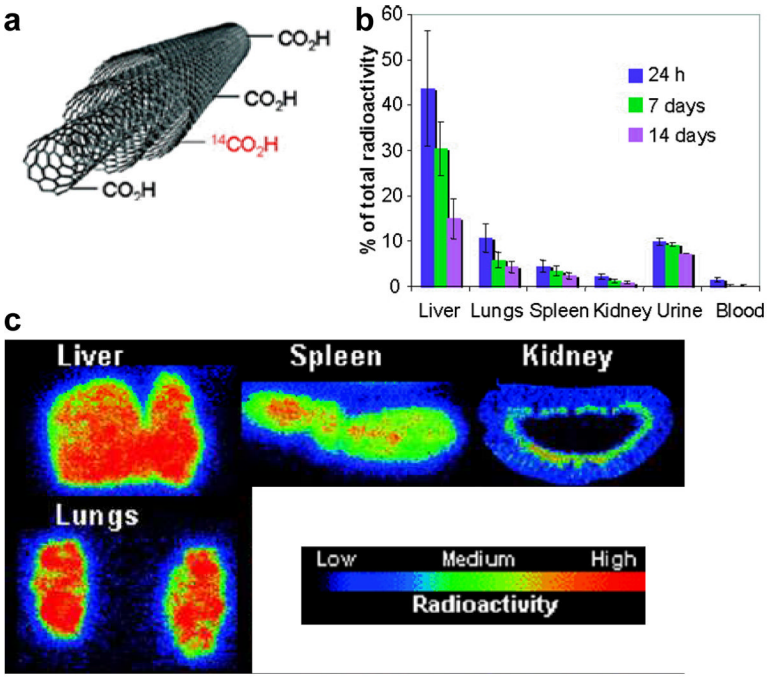

Fig. 2.

a Schematic structure of ^{14}C-labeled MWNTs. **b** Biodistribution of ^{14}C-labeled MWNTs at different time points after intravenous injection. **c** Autoradiography images of mouse liver, lungs, spleen, and kidney at 24 h post-injection of ^{14}C-labeled MWNTs. Adapted with permission from reference [38].

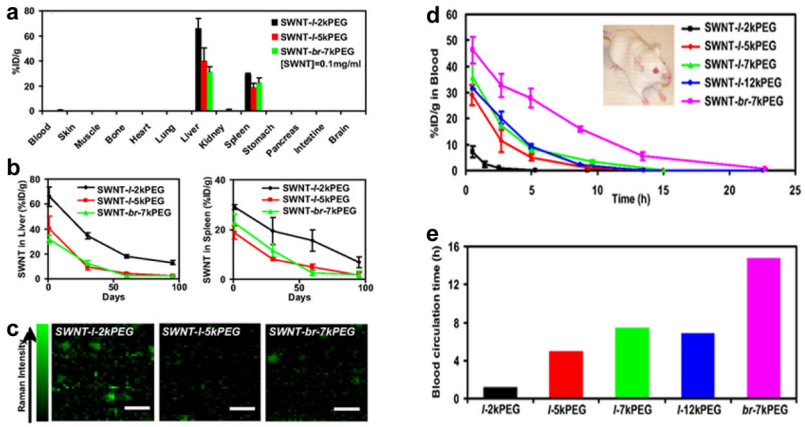

Fig. 3.

a Biodistribution of SWNT conjugated with different PEG chains at 1 day post-injection, as measured by Raman spectroscopy. l: linear; br: branched. **b** The retention profile of SWNT in mouse liver and spleen over a period of three months. **c** Raman images of liver slices from mice treated with SWNTs functionalized with different PEG chains. **d** Blood concentration of intravenously injected SWNTs functionalized with different PEG chains, as measured by Raman imaging. **e** Blood circulation time of SWNTs functionalized with different PEG chains. Adapted with permission from reference [16].

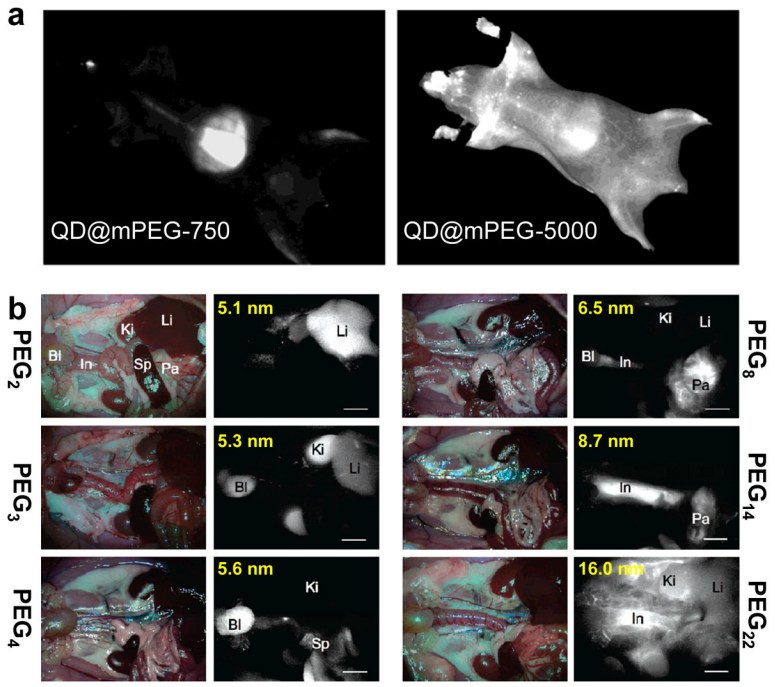

Fig. 4.

a *In vivo* whole body fluorescence imaging of QD@mPEG-750 and QD@mPEG-5000 at 1 h post-injection into mice. **b** In situ fluorescence imaging of intravenously injected QDs coated with varied length of PEG chains (2–22 ethylene glycol units). The hydrodynamic diameters of the QDs are also shown (ranging from 5.1 to 16.0 nm). Bl: bladder; In: intestine; Ki: kidney; Li: liver; Pa: pancreas; Sp: spleen. Adapted with permission from references [79, 81].

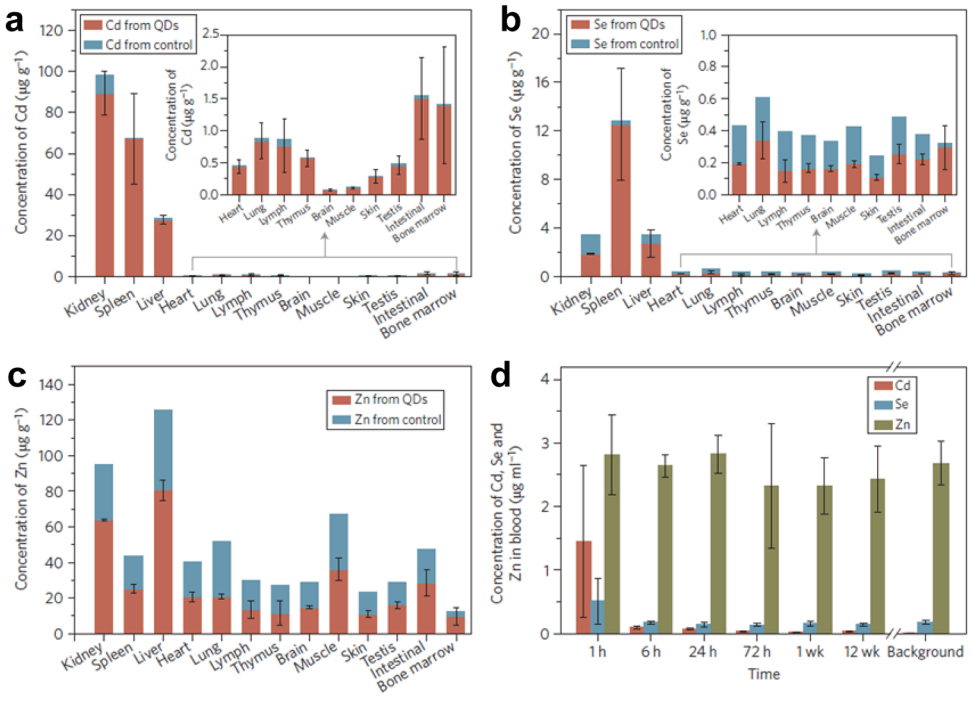

Fig. 5.

ICP-MS analysis of the major organs of treated and control rhesus macaques at day 90 after intravenous injection of CdSe@CdS@ZnS QDs, showing the biodistribution of cadmium (**a**), selenium (**b**), and zinc (**c**). **d** Blood clearance profile of QDs *in vivo*. Adapted with permission from reference [97].

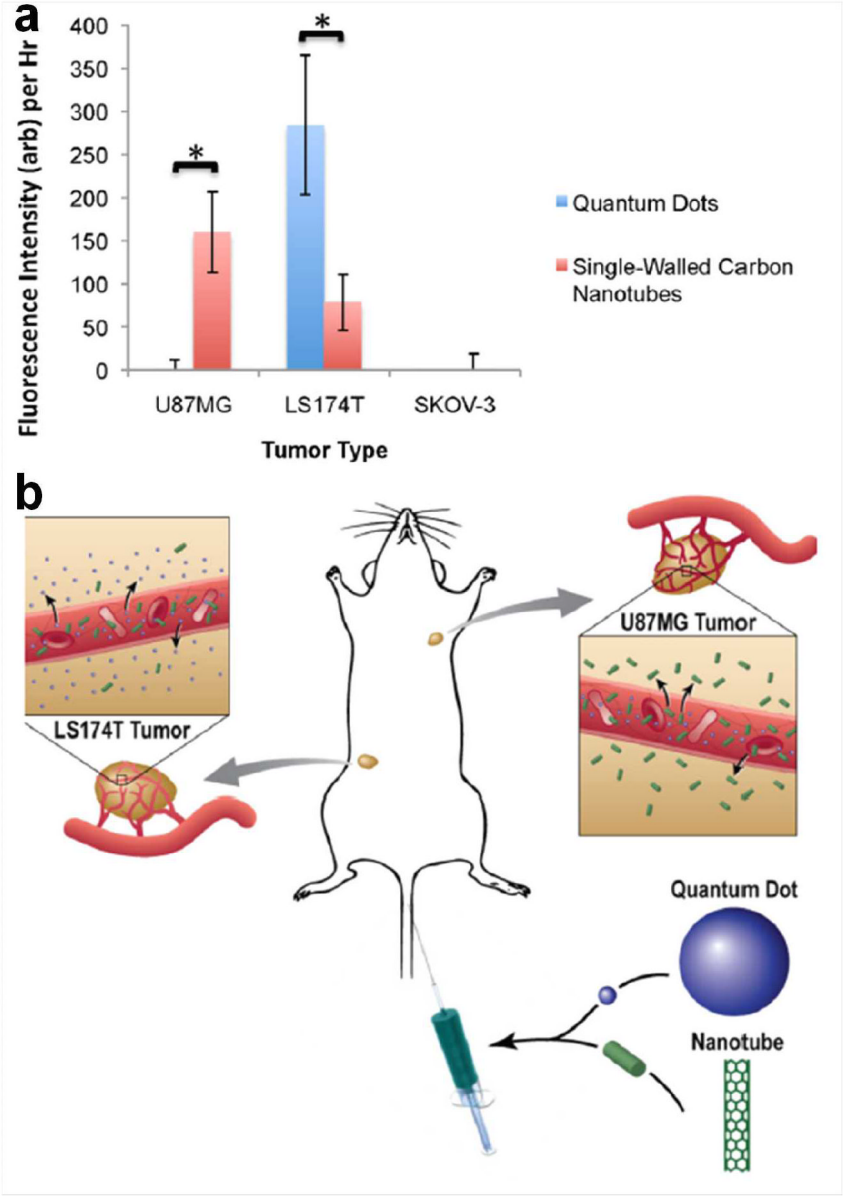

Fig. 6.

Extravasation of QDs and SWNTS from the vasculature of murine tumor models. **a** Extravasation of QDs is compared with that of SWNTS for each tumor type. **b** A schematic illustration showing that QDs extravasate from the LS174T tumor but not the U87MG tumor, whereas SWNTS extravasate from the U87MG tumor but only minimally from the LS174T tumor. Adapted with permission from reference [104].